IOP Conf. Series: Journal of Physics: Conf. Series **994** (2018) 012017 doi:10.1088/1742-6596/994/1/012017

Ambiguities and completeness of SAS data analysis: investigations of apoferritin by SAXS/SANS EID and SEC-SAXS methods

D V Zabelskii[1,2,α], A V Vlasov[1,3,α], Yu L Ryzhykau[1], T N Murugova[1,4], M Brennich[5], D V Soloviov[1,4,6], O I Ivankov[1,4,7], V I Borshchevskiy[1], A V Mishin[1], A V Rogachev[1,4], A Round[8], N A Dencher[1,9], G Büldt[1], V I Gordeliy[1,2,10] and A I Kuklin[1,4]*

[1]Research center for molecular mechanisms of aging and age-related diseases, Moscow Institute of Physics and Technology, Dolgoprudny, Russian Federation
[2]Institut de Biologie Structurale, J.-P. Ebel, Université Grenoble Alpes-CEA-CNRS, Grenoble, F-38000, France
[3]Institute of Crystallography, RWTH Aachen University, Germany
[4]Joint Institute for Nuclear Research, Dubna, Russian Federation
[5]European Molecular Biology Laboratory, Grenoble Outstation, CS 90181, 71 Avenue des Martyrs, 38042, Grenoble Cedex 9, CS 90181, France
[6]Shevchenko National University of Kyiv, Kyiv, Ukraine
[7]Institute for safety problems of nuclear power plants NAS of Ukraine, Kyiv, Ukraine
[8]European X-Ray Free-Electron Laser Facility GmbH at Amtsgericht Hamburg, HRB 111165
[9]CSI Organic Chemistry and Biochemistry, Technische Universität Darmstadt, Darmstadt, D-64287, Germany
[10]Institute of Complex Systems: Structural Biochemistry (ICS-6), Research Centre Jülich, Jülich, 52425, Germany,
[α]-equal contribution
kuklin@nf.jinr.ru

Abstract. The method of small angle scattering (SAS) is widely used in the field of biophysical research of proteins in aqueous solutions. Obtaining low-resolution structure of proteins is still a highly valuable method despite the advances in high-resolution methods such as X-ray diffraction, cryo-EM etc. SAS offers the unique possibility to obtain structural information under conditions close to those of functional assays, i.e. in solution, without different additives, in the mg/mL concentration range. SAS method has a long history, but there are still many uncertainties related to data treatment. We compared 1D SAS profiles of apoferritin obtained by X-ray diffraction (XRD) and SAS methods. It is shown that SAS curves for X-ray diffraction crystallographic structure of apoferritin differ more significantly than it might be expected due to the resolution of the SAS instrument. Extrapolation to infinite dilution (EID) method does not sufficiently exclude dimerization and oligomerization effects and therefore could not guarantee total absence of dimers account in the final SAS curve. In this study, we show that EID SAXS, EID SANS and SEC-SAXS methods give complementary results and when they are used all together, it allows obtaining the most accurate results and high confidence from SAS data analysis of proteins.

1. Introduction

Small-angle scattering (SAS) is a powerful technique for investigating large-scale structures at scales from 10Å to 10^4Å and is widely used in biology and material science [1–20] especially for investigations of complexes [21–26] and large structures [27–29], Consequently, the question of quantitative characterization of these structures becomes extremely important. In structural biology, small-angle X-ray and neutron scattering (SAXS and SANS) are mostly used to determine integral structural parameters of biomolecules such as radius of gyration, scattering volume or aggregation parameters. SAXS and SANS allow one to recover three-dimensional shape from one-dimensional scattering pattern by dummy atom modelling [30]. These approaches require high purity and monodispersity of samples in order to exclude clustering effects by using standard sample preparation protocols and data processing methods such as extrapolation to infinite dilution (EID). The EID method uses extrapolation of I(q) curves for different concentrations of the protein to zero concentration for creating idealized scattering curve [31]. The method works well for excluding of structure factor effects. In case there are dimers or aggregates and the dependency on concentration is sophisticated, we suggest using small angle X-ray scattering method combined with size-exclusion gel-chromatography (SEC-SAXS) method. SEC-SAXS uses on-line high-pressure liquid chromatography (HPLC) system coupled with SAXS instrument that enables direct SAXS measurements of chromatographic sample fractions. Originally this method was developed to allow measurements of unstable and aggregating samples, but it can also be used for stable proteins [32–39].

In this investigation, we show dummy atom models reconstructed from the scattering curves. We use apoferritin due to its simplicity, stability and highly spherical shape [40–42]. Apoferritin is an iron depleted form of ferritin which is well known for its important role as main iron storage [43–45]. In accordance with X-ray crystallography data, apoferritin consists of 24 subunits forming a quasi-spherical core shell with a cavity inside [46] and several intersubunit channels that communicate between the interior of the molecule and external environment. Apoferritin may encapsulate small molecules, making it an interesting system for drug delivery [41,47–49]. Moreover, ferritin could be a candidate for a marker of cancer and/or biological age [50] or has a biotechnical implementations like some other proteins such as rhodopsins etc. [51,52]. However, crystallographic structure of the protein state can be influenced by crystallization conditions and crystal packing. Usually authors do not distinguish the influence of the structure factor effects and the effects of oligomerization, taking into account the quadratic dependence of the scattering intensity on the volume of the object under study. Therefore, SAS is an important approach that could be used to determine structural parameters of apoferritin under native conditions.

Apoferritin 3D dummy atom modelling was already done in both small angle X-ray (SAXS) and neutron (SANS) scattering experiments, using EID method to exclude clustering effects [53].

However, the EID method can be insufficient to obtain an idealized monomer SAXS curve with confidence. The quality of SAXS data throughout the full Q-range plays crucial role in data processing and may seriously influence final models and conclusions if not treated correctly.

The aim of this study is a comparative analysis of structural parameters of proteins in solution and in crystal using as an example the protein apoferritin. This requires the greatest possible resolution and elimination of the structure and oligomeric factors. As it was mentioned above, different methods provide different results, which might also depend on the oligomeric factor and concentration of the protein.

2. Materials and Methods

2.1. SEC-SAXS experimental setup and sample description

Horse spleen apoferritin was purchased from Sigma-Aldrich Chemie GmbH (Product number A3660). Storage buffer (50% glycerol and 0.075 M NaCl) was replaced with buffer (200 mM NaCl and 20 mM

Tris, pH=7.5) by dialysis in 1L of the buffer. After dialysis, the protein was applied to Superdex 200 (S200 GL 10/300, GE Healthcare) size-exclusion column, which was connected to on-line HPLC system (LC-20ADXR, Shimadzu) attached directly to the sample-inlet valve of the BM29 sample capillary [39,54]. 500 µL of 8.8 mg/mL protein solution were injected onto the column (Superdex 200 10/300 GL, GE Healthcare). Buffers were degassed and the column was equilibrated with 1.5 column volumes of buffer. A flow rate of 0.5 ml/min at room temperature was used and the baseline was monitored. All data from the run were collected at a wavelength of 0.99 Å using a sample-to-detector distance (PILATUS 1M, DECTRIS) of 2.876 meters corresponding to an effective Q range of 0.008–0.45Å^{-1}. Approximately 1200 frames (1 frame per 2s) were collected per 40 min sample run and initial data processing was performed automatically using the EDNA pipeline [47,55], generating radially integrated, calibrated and normalized one-dimensional profiles for each frame. All frames were compared with the initial frame and matching frames were merged to create the reference buffer automatically by the EDNA software.

Frames with a consistent Rg from the peak scattering intensity were manually merged to get a single averaged frame corresponding to the scattering of SEC purified monomer fraction. Specifically, 20 frames corresponding to the monomer peak were merged and used for all further data processing and model fitting.

2.2. SEC purification

Horse spleen apoferritin was purified as a soluble protein by SEC-SAXS experimental setup. In Fig.1 two partially resolved peaks represent different fractions of apoferritin in solution. In SEC method fractions with higher molecular weight elutes first, therefore peak fraction “B” corresponds to oligomer fraction that is in a good agreement with Rg and I(0) data. Peak fraction “A” is the apoferritin monomer fraction with high purity and monodispersity that is controlled by Rg data. Frames used for creating the idealized SAXS curve correspond the peak monomer fractions with the highest I(0) and absorbance (range limited by the vertical dash lines in Fig. 1). However, only 20 peak frames were taken for merging due to possible concentration effects that may affect the final curve. Difference in effective concentrations and gyration radii between frames used for merging is less than 10%. We note that more frames can be used for averaging, although, this will give insufficient effect on the quality of the scattering curve.

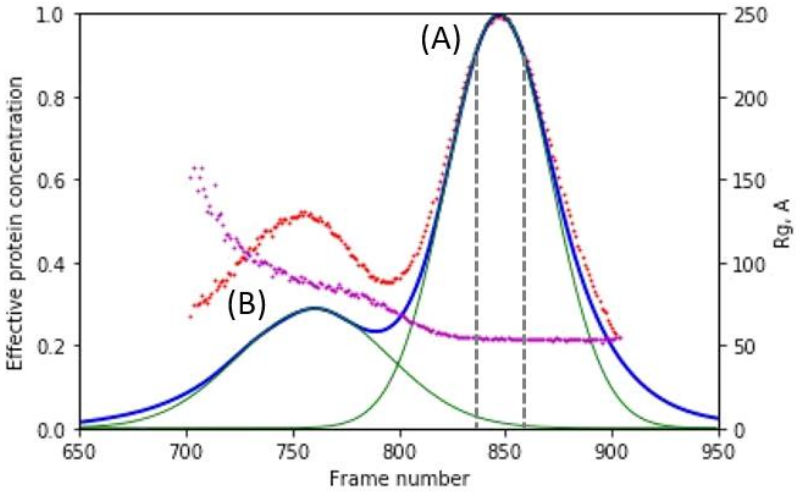

Figure 1. The curve of normalized absorbance at λ = 280 nm (blue line) corresponds to effective protein concentration, SAXS intensity at zero angle is represented in red dots. Gyration radii are represented in purple dots. Gaussian fits of two peaks are coloured in green lines. Vertical dash lines represent range of frames used for merging into final SAXS curve of the protein.

2.3. SAS data processing

Here is a brief description of data treatment, a full description can be found elsewhere, for example, in [53]. For monodisperse particles, the scattering intensity is written as:

$$I(Q) = nS(Q)|F(Q)|^2 \qquad (1)$$

where Q is the scattering vector, n is a concentration, S(q) is the structure factor and F(q) the form factor of the proteins. EID method is extrapolation I(q) vs q^2 to zero for series of scattering curves for different concentrations and gives zero concentration curve free of clustering effects. Scattering volume can be determined by [53]:

$$V = \frac{2\pi^2 I(0)}{\int Q^2 I(Q) dQ} \qquad (2)$$

For shape determination the protein is represented by a set of homogeneous atoms (beads) where the difference between the computed scattering and the experimental data is minimized [56]. Algorithm considers both scattering intensity pattern and pair-distance distribution function during operation. Best models with connectivity are averaged during processing to give the final *ab initio* model.

In this investigation integral parameters of apoferritin are calculated by ATSAS and visualised with SasView software packages [57,58]. The pair-distance distribution function is obtained with the program PRIMUS using GNOM [59]. 3D ab-initio model of apoferritin monomer is calculated by the DAMMIF program from the ATSAS-online platform.

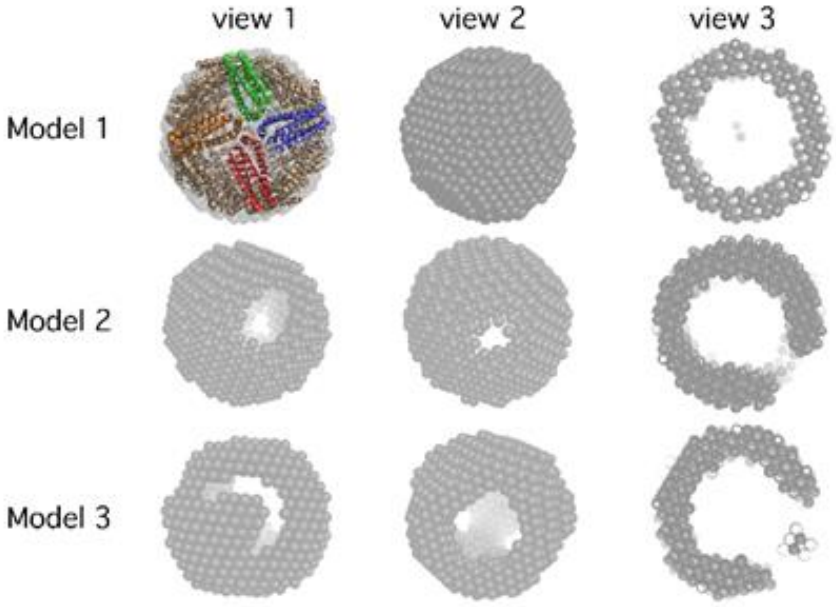

Figure 2. Projections of apoferritin dummy atom models reconstructed from SAXS and SANS data. Forward and backward projections and central section of SEC-SAXS, EID SAXS and EID SANS dummy atom models are presented as Model 1, Model 2 and Model 3 respectively. Projection of SEC-SAXS model with overlaid PDB structure (PDB code: 2W0O) is presented.

It is worth pointing out that we did a number of EID SAXS experiments and only the experiments that were done with specific pH and salt conditions gave results similar to those obtained by SEC-SAXS. For example, such a good correspondence between Rg obtained from SEC-SAXS and EID SAXS became possible only at very specified pH and salt conditions (150 mM NaCl and 5 mM Na_2HPO_4, pH = 7.3) [60], but in other experiments the discrepancies in Rg was more than 10%. It proves that if there is a sample that is not possible to be measured by SEC-SAXS (for example colloidal or magnetic particles

solutions, dendrimers, powders, etc.), it strongly requires a very specific buffer conditions under which the aggregation diminishes and it became possible to apply EID SAXS.

3. Results and Discussion

Here we compare scattering data obtained by SEC-SAXS method with data obtained by the EID method from our previous SAXS and SANS experiments also. The full description of these experiments is available in [60]. During the subsequent analysis of scattering data obtained with EID method are denoted as EID SAXS and EID SANS data for X-ray and neutron data, respectively.

3.1. Core shell model analysis and pair-distribution function

Dummy atom models calculated during processing the SEC-SAXS curve are shown in Fig. 3 and core shell model fit of SAXS curve is shown in Fig. 4. In particular, the scattering curve is fitted by a core shell model from SasView program [58] at q-range 0.007-0.305 $Å^{-1}$ and structural analysis using ATSAS package was done [57]. Apoferritin PDB structure (PDB code: 2W0O) was processed by PEPSI-SAXS program and fitted to experimental data (Fig. 5) [61]. The results of chi-squared goodness of fit test are $chi^2 = 47.6$ and $chi^2 = 51.1$ for SEC-SAXS and EID SAXS models, respectively. We suggest this result is mainly due to poor fit in the Q-region near the tails of the curves. Such divergence may correspond to higher packing of crystal apoferritin in comparison to apoferritin in solution. PEPSI-SAXS fit is presented on Kratky plot (IQ^2 vs Q) (Fig. 5) and Guinier plot (ln(I) vs Q^2) (Fig. 6). The radius of gyration and scattering volume of apoferritin were directly estimated with PRIMUS. Comparing the previous results obtained by SANS and SAXS EID [60] and SEC-SAXS, it is shown that parameters such as radius of gyration, inner and outer radii are almost the same for both methods. However, the scattering volume gives different results for all models. Possible reasons of the difference obtained in SANS and SAXS experiments may be caused by the hydration shell, which is not detected by SANS, or because of hydrogen/deuterium exchange or sample impurities, for example, as reported in [62]. In any case, the difference between inner radii of apoferritin obtained by SAXS and SANS is similar to the difference between outer radii obtained by SAXS and SANS (~2.5 Å). This fact could imply that the same reasons are responsible for the difference in inner and outer apoferritin compartments. Difference in volumes obtained in SAXS EID and SEC-SAXS could occur due to the reasons mentioned above or aggregation effects or structural ordering [63]. It is known that the EID method could not exclude oligomerization and therefore scattering volume will give overestimated results.

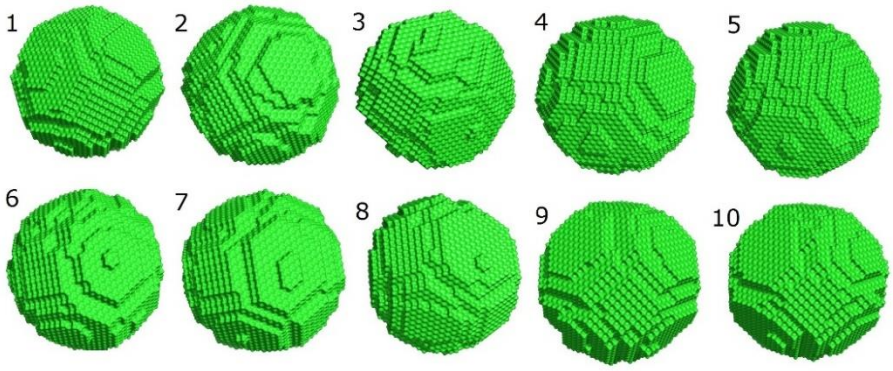

Figure 3. Dummy atom models calculated during processing SEC-SAXS curve used for averaging into final model. All intermediate models have nearly spherical form and cavity inside.

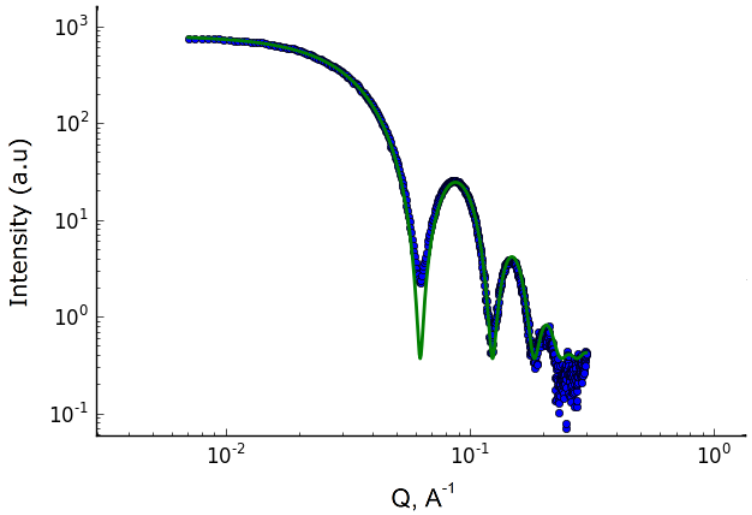

Figure 4. SEC-SAXS scattering curve is presented in blue dots, a curve of core shell model fit is presented in green line. Q-range is 0.006 – 0.2 1/Å

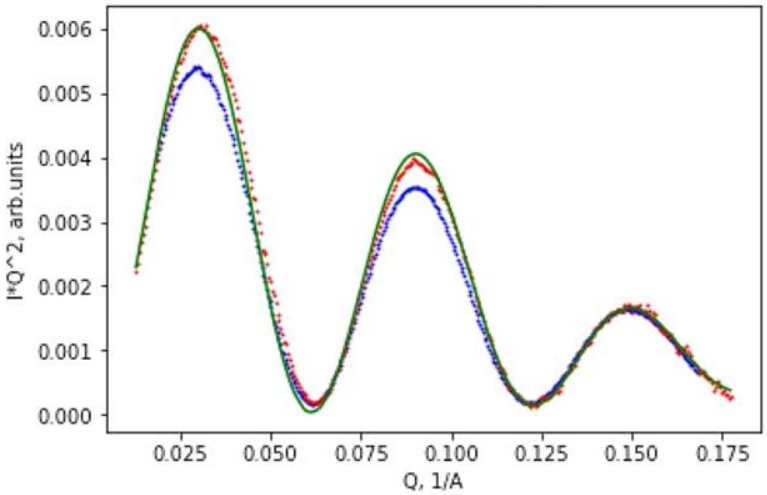

Figure 5. Kratky plot (IQ^2 versus Q) of SEC-SAXS and EID SAXS curves overlaid with PEPSI-SAXS fit. Blue dots represent EID, red dots – SEC-SAXS experimental curves. Green curve represents PEPSI-SAXS fit of experimental curves. Curves presented within the Q-range 0.01 - 0.175 1/Å.

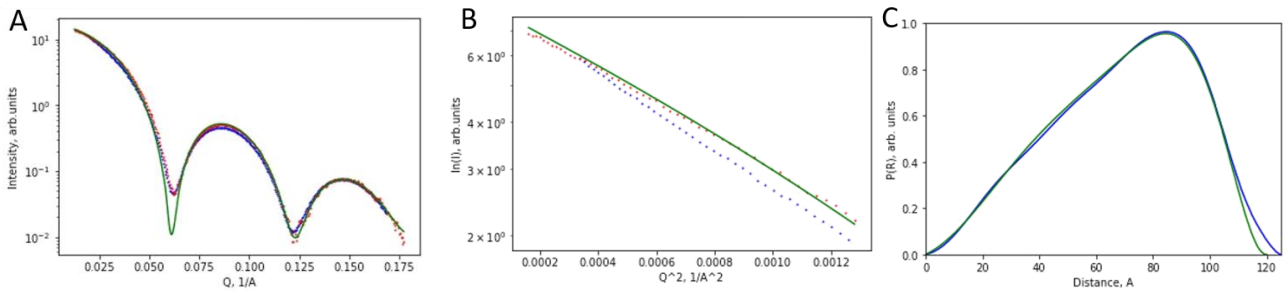

Figure 6. Intensity (A) and Guinier (B) and pair-distance plots of SEC-SAXS (red dots) and EID SAXS (blue dots) are presented and overlaid with CRYSOL fit (green line). Curves presented on Intensity plot (A) within Q-range 0.02 – 0.175 1/Å. Curves on Guinier plot (B) (ln(I) versus Q2) are presented within Q-range 0.01 – 0.035 1/Å, that includes Q-region corresponding to QRg < 1 condition. Distance distribution functions (C) of corresponding SEC-SAXS (green line) and EID SAXS (blue line) curves are presented.

The pair-distance distribution function P(r) was obtained by indirect Fourier transformation of apoferritin experimental SAXS data using GNOM program and is shown in Fig. 6. This function allows the calculation of the largest dimension in a particle. In particular, for apoferritin monomer D_{max} is 120 Å that almost corresponds to the outer diameter in terms of spherical shell model (D = 123 Å) and previously obtained results (D = 125 Å). We assume that the difference between D_{max} and D could appear because apoferritin shell is not completely spherical in solution as it is not completely rigid.

3.2. Core dummy atom model analysis

Projections of apoferritin low-resolution 3D models are shown in Fig 2. All presented models have almost spherical surfaces with cavities that corresponds to the literature data [62] and PDB structure (2W0O). Dummy atom model obtained by SEC-SAXS corresponds to PDB (Fig. 2). Models obtained by EID SAXS and SANS demonstrate statistical artefacts of data analysis process (cavities in surface). The difference to the data between the fit of the full sphere and a sphere with the hole to the data is minimal. The hole is a statistical result of the random seed. In any models with the holes during the merging process the hole will be align and persist. Despite PEPSI-SAXS fit for both SEC-SAXS and EID SAXS data results in similar curves and both curves lead to almost similar gyration radius, the 1D curves show slight difference and predict different scattering volume. We think this difference may show that SEC-SAXS is better for excluding clustering effects than EID SAXS and SEC-SAXS does not match the scattering volume (predicted by PEPSI-SAXS) because PEPSI-SAXS does not take into account thermal fluctuations of apoferritin under native conditions. We also note that the SAXS dummy atom model predicts slightly larger outer radii and scattering volume than the SANS model. It might be explained by deuterium substitution effect and difference in scattering densities obtained by SAXS and SANS [53].

Conclusion

We have determined a 3D ab initio model of apoferritin using SEC-SAXS and compared this model with PDB and models obtained with EID SAXS and EID SANS. Both EID and SEC-SAXS methods give representatives and complementary results, so whenever possible SEC-SAXS should be undertaken as well as EID (for higher concentrations) and comparisons of the data should be made to validate the data analysis process and increase confidence in the models and conclusions made from the data. We assume that data obtained by SEC-SAXS may be more suitable than EID SAXS data for making SAXS combined with X-ray diffraction or cryo-EM data analysis.

Acknowledgments
We acknowledge the European Synchrotron Radiation Facility for providing synchrotron radiation facilities. We thank ESRF structural biology group for their assistance during the experiments. The investigation used the platforms of the Grenoble Instruct Centre (ISBG; UMS 3518 CNRS-CEA-UJF-EMBL). We also thank Russian Science Foundation (grant No. 16-15-00242); FRISBI (grant No. ANR-10-INSB-05-02); GRAL within the Grenoble Partnership for Structural Biology (PSB) (grant No. ANR-10-LABX-49-01); CEA(IBS) and HGF(FZJ) (contract No. CEA(IBS) – HGF(FZJ) STC 5.1 specific agreement).

References
[1] Hura G L, Menon A L, Hammel M, Rambo R P, Poole F L, Tsutakawa S E, Jenney F E, Classen S, Frankel K A, Hopkins R C, Yang S-J, Scott J W, Dillard B D, Adams M W W and Tainer J A 2009 Robust, high-throughput solution structural analyses by small angle X-ray scattering (SAXS). *Nat. Methods* **6** 606–12
[2] Kuklin A I, Islamov A K and Gordeliy V I 2005 Scientific Reviews: Two-Detector System for Small-Angle Neutron Scattering Instrument *Neutron News* **16** 16–8
[3] Rambo R P and Tainer J A 2013 Accurate assessment of mass, models and resolution by small-angle scattering. *Nature* **496** 477–81
[4] Kuklin A I, Rogachev A V, Soloviov D V, Ivankov O I, Kovalev Y S, Utrobin P K, Kutuzov S A, Soloviev A G, Rulev M I and Gordeliy V I 2017 Neutronographic investigations of supramolecular structures on upgraded small-angle spectrometer YuMO *J. Phys. Conf. Ser.* **848** 12010
[5] Bulavin L A, Gordeliy V I, Ivan'kov O I, Islamov A K and Kuklin A I 2010 Neutron studies of the NaBr impurity influence on micelle formation in the heay water-tetradecyltrimethylammonium bromide systems *Ukr. J. Phys.* **55** 288–92
[6] Bulavin L A, Ivankov O I, Islamov A K and Kuklin A I 2010 Structure transformations in the triple liquid system tetradecyltrimethylammonium bromide-D2O-NaBr *Ukr. J. Phys.* **55** 410–4
[7] Rogachev A V, Cherny A Y, Ozerin A N, Muzafarov A M, Atatarinova E, Islamov A K, Gordeliy V I and Kuklin A I 2008 Revealing inner structure of the polycarbosilane dendrimers from small-angle neutron scattering data *J. Phys. Conf. Ser.* **129** 12041
[8] Anghel L, Balasoiu M, Ishchenko L A, Stolyar S V, Rogachev A V, Kurkin T S, Kuklin A I, Raikher Y L, Iskhakov R S and Arzumanian G M 2012 SAXS Studies of Ultrasonicated Dispersions of Biomineral Particles Produced by <i>Klebsiella oxytoca</i> *Solid State Phenom.* **190** 621–4
[9] Anitas E M, Cherny A Y, Osipov V A and Kuklin A I 2014 Small-angle scattering from three-phase systems: Investigation of the crossover between mass fractal regimes *J. Phys. Conf. Ser.* **490** 12028
[10] Gibhardt H, Haramagatti C R, Islamov A K, Ivankov O I, Kuklin A I and Eckold G 2015 Ordering Phenomena in Surfactant Systems: From Micellar Solutions to Gel and Crystalline Phases *Zeitschrift für Phys. Chemie* **229** 1869–85
[11] Soloviov D, Zabashta Y, Bulavin L, Olexandr I, Gordeliy V and Kuklin A 2014 Changes in the Area per Lipid Molecule by P-V-T and SANS Investigations *Macromol. Symp.* **335** 58–61
[12] Solov'ev D V., Kuklin A I, Utrobin P K, Ozerin A N, Kurkin T S, Ivan'kov O I, Bulavin L A and Gordelii V I 2011 X-ray scattering and volumetric P-V-T studies of the dimyristoylphosphatidylcholine-water system *J. Surf. Investig. X-ray, Synchrotron Neutron Tech.* **5** 7–10
[13] Balasoiu-Gaina A-M, Balasoiu M, Ivankov O, Soloviov D, Lysenko S, Stan C, Lupu N, Creanga D and Kuklin A 2017 Structural analysis of aqueous ferrofluids with cobalt ferrite particles stabilized with lauric acid and sodium n-dodecyl sulphate *J. Phys. Conf. Ser.* **848**

12026
[14] Shibaev A V, Makarov A V, Aleshina A L, Rogachev A V, Kuklin A I and Philippova O E 2017 Structure and oil responsiveness of viscoelastic fluids based on mixed anionic/cationic wormlike surfactant micelles *J. Phys. Conf. Ser.* **848** 12019
[15] Shibaev A V, Kuklin A I and Philippova O E 2017 Effect of polymer on the arrangement of mixed anionic/cationic wormlike surfactant micelles revealed by SANS *J. Phys. Conf. Ser.* **848** 12006
[16] Dragolici A C, Balasoiu M, Orelovich O L, Ionascu L, Nicu M, Soloviov D V, Kuklin A I, Lizunov E I and Dragolici F 2017 CEM V based special cementitious materials investigated by means of SANS method. Preliminary results *J. Phys. Conf. Ser.* **848** 12024
[17] Soloviov D V, Bulavin L A, Gordeliy V I, Gorshkova Y E, Ivankov O I, Kovalev Y S, Kuklin A I and Nikolaenko T Y Neutron Scattering Investigations of the Lipid Bilayer Structure Pressure Dependence *Nucl. Phys. At. energy* **13** 83–8
[18] Egorov V V, Zabrodskaya Y A, Lebedev D V, Gorshkov A N and Kuklin A I Structural features of the ionic self-complementary amyloidogenic peptide *J. Phys. Conf. Ser.* **848** 12022
[19] Loiko P A, Rachkovskaya G E, Skoptsov N A, Arzumanyan G M, Kulik M, Kuklin A I, Zakharevich G B, Yumashev K V. and Mateos X 2017 Mechanisms of Up-Conversion Luminescence in Glass-Ceramics Containing Er:PbF2 Nanocrystals *J. Appl. Spectrosc.* **84** 194–201
[20] Kulvelis Y V, Ivanchev S S, Primachenko O N, Lebedev V T, Marinenko E A, Ivanova I N, Kuklin A I, Ivankov O I and Soloviov D V. 2016 Structure and property optimization of perfluorinated short side chain membranes for hydrogen fuel cells using orientational stretching *RSC Adv.* **6** 108864–75
[21] Murugova T N, Gordeliy V I, Kuklin A I, Kovalev Y S, Yurkov V I, Nurenberg A, Islamov A K and Yaguzhinskii L S 2006 Detection of new double-membrane structures in native mitochondria by the method of small-angle neutron scattering *Biophysics (Oxf).* **51** 882–6
[22] Murugova T N, Gordeliy V I, Kuklin A I, Solodovnikova I M and Yaguzhinsky L S 2007 Study of three-dimensionally ordered structures of intact mitochondria by small-angle neutron scattering *Crystallogr. Reports* **52** 521–4
[23] Murugova T N, Solodovnikova I M, Yurkov V I, Gordeliy V I, Kuklin A I, Ivankov O I, Kovalev Y S, Popov V I, Teplova V V. and Yaguzhinsky L S 2011 Potentials of Small-angle Neutron Scattering for Studies of the Structure of "Live" Mitochondria *Neutron News* **22** 11–4
[24] Zabrodskaya Y A, Lebedev D V., Egorova M A, Shaldzhyan A A, Shvetsov A V., Kuklin A I, Vinogradova D S, Klopov N V., Matusevich O V., Cheremnykh T A, Dattani R and Egorov V V. 2018 The amyloidogenicity of the influenza virus PB1-derived peptide sheds light on its antiviral activity *Biophys. Chem.* **234** 16–23
[25] Selivanova O M, Surin A K, Ryzhykau Y L, Glyakina A V., Suvorina M Y, Kuklin A I, Rogachevsky V V. and Galzitskaya O V. 2018 To Be Fibrils or To Be Nanofilms? Oligomers Are Building Blocks for Fibril and Nanofilm Formation of Fragments of Aβ Peptide *Langmuir* **34** 2332–43
[26] Ryzhykau Y, Nikolaev M, Zabelskii D, Kuklin A and Gordeliy V 2017 Trimers of dimers of SRII/HtrII full complex. Small angle scattering structural investigation *FEBS J.* **284** 154
[27] Kadochnikov V V., Egorov V V., Shvetsov A V., Kuklin A I, Isaev-Ivanov V V. and Lebedev D V. 2016 Modeling of conformational transitions of fibrillogenic peptide, homologous to beta-domain of human alpha-lactalbumin *Crystallogr. Reports* **61** 98–105
[28] Egorov V V., Shaldzhyan A A, Gorshkov A N, Zabrodskaya Y A, Lebedev D V., Kuklin A I, Ksenofontova O I, Shvetsov A V., Vasin A V., Tsybalova L M and Isaev-Ivanov V V. 2016 On the structural features of influenza A nucleoprotein particles from small-angle X-ray scattering data *J. Surf. Investig. X-ray, Synchrotron Neutron Tech.* **10** 322–5
[29] Schmidt A E, Shvetsov A V., Kuklin A I, Lebedev D V., Surzhik M A, Sergeev V R and Isaev-Ivanov V V. 2016 Small-angle scattering study of Aspergillus awamori glycoprotein

glucoamylase *Crystallogr. Reports* **61** 149–52
[30] Franke D and Svergun D I 2009 DAMMIF , a program for rapid ab-initio shape determination in small-angle scattering *J. Appl. Crystallogr.* **42** 342–6
[31] Zimm B H 1948 The Scattering of Light and the Radial Distribution Function of High Polymer Solutions *J. Chem. Phys.* **16** 1093
[32] Lambright D, Malaby A W, Kathuria S V., Nobrega P R, Osman B, Matthews R C, Muthurajan U, Luger K, Chopra R, Irving T C and Chakravarthy S 2013 COMPLEMENTARY TECHNIQUES ENHANCE THE QUALITY AND SCOPE OF INFORMATION OBTAINED FROM SAXS *Trans. Am. Crystallogr. Assoc.* **44**
[33] Mathew E, Mirza A, Menhart N and IUCr 2004 Liquid-chromatography-coupled SAXS for accurate sizing of aggregating proteins *J. Synchrotron Radiat.* **11** 314–8
[34] David G, Pérez J and IUCr 2009 Combined sampler robot and high-performance liquid chromatography: a fully automated system for biological small-angle X-ray scattering experiments at the Synchrotron SOLEIL SWING beamline *J. Appl. Crystallogr.* **42** 892–900
[35] Graewert M A, Franke D, Jeffries C M, Blanchet C E, Ruskule D, Kuhle K, Flieger A, Schäfer B, Tartsch B, Meijers R and Svergun D I 2015 Automated pipeline for purification, biophysical and x-ray analysis of biomacromolecular solutions. *Sci. Rep.* **5** 10734
[36] Watanabe Y and Inoko Y 2009 Size-exclusion chromatography combined with small-angle X-ray scattering optics *J. Chromatogr. A* **1216** 7461–5
[37] Grant T D, Luft J R, Wolfley J R, Tsuruta H, Martel A, Montelione G T and Snell E H 2011 Small angle X-ray scattering as a complementary tool for high-throughput structural studies *Biopolymers* **95** 517–30
[38] Acerbo A S, Cook M J, Gillilan R E and IUCr 2015 Upgrade of MacCHESS facility for X-ray scattering of biological macromolecules in solution *J. Synchrotron Radiat.* **22** 180–6
[39] Brennich M E, Round A R and Hutin S 2017 Online Size-exclusion and Ion-exchange Chromatography on a SAXS Beamline. *J. Vis. Exp.*
[40] Russo C J and Passmore L A 2014 Ultrastable gold substrates for electron cryomicroscopy. Supplementary *Science* **346** 1377–80
[41] Heger Z, Skalickova S, Zitka O, Adam V and Kizek R 2014 Apoferritin applications in nanomedicine. *Nanomedicine (Lond).* **9** 2233–45
[42] Jurado R, Castello F, Bondia P, Casado S, Flors C, Cuesta R, Dominguez-Vera J M, Orte A and GALVEZ N 2016 Apoferritin Fibers: a New Template for 1D Fluorescent Hybrid Nanostructures *Nanoscale* 9648–56
[43] Andrews S C 1998 Iron Storage in Bacteria *Adv. Microb. Physiol.* **40** 281–351
[44] Crichton R R and Ward R J 1998 Iron homeostasis. *Met. Ions Biol. Syst.* **35** 633–65
[45] Massover W H 1993 Ultrastructure of ferritin and apoferritin: A review *Micron* **24** 389–437
[46] Ford G C, Harrison P M, Rice D W, Smith J M, Treffry A, White J L and Yariv J 1984 Ferritin: design and formation of an iron-storage molecule. *Philos. Trans. R. Soc. Lond. B. Biol. Sci.* **304** 551–65
[47] Kanekiyo M, Wei C-J, Yassine H M, McTamney P M, Boyington J C, Whittle J R R, Rao S S, Kong W-P, Wang L and Nabel G J 2013 Self-assembling influenza nanoparticle vaccines elicit broadly neutralizing H1N1 antibodies *Nature* **499** 102–6
[48] Geninatti Crich S, Cadenazzi M, Lanzardo S, Conti L, Ruiu R, Alberti D, Cavallo F, Cutrin J C and Aime S 2015 Targeting ferritin receptors for the selective delivery of imaging and therapeutic agents to breast cancer cells *Nanoscale* **7** 6527–33
[49] Sahandi Zangabad P, Karimi M, Mehdizadeh F, Malekzad H, Ghasemi A, Bahrami S, Zare H, Moghoofei M, Hekmatmanesh A and Hamblin M R 2017 Nanocaged platforms: modification, drug delivery and nanotoxicity. Opening synthetic cages to release the tiger *Nanoscale* **9** 1356–92
[50] Stevens R G, Jones D Y, Micozzi M S and Taylor P R 1988 Body Iron Stores and the Risk of Cancer *N. Engl. J. Med.* **319** 1047–52

[51] Vlasov A, Kovalev Y, Ryzhykau Y, Frolov F, Zinovev E, Rogachev A, Kuklin A and Gordeliy V 2016 Light-induced electrical properties of bacteriorhodopsin in purple membranes *FEBS J.* **283** 218
[52] Vlasov A V, Kovalev Y S, Utrobin P K, Ryzhykau Y L, Frolov F V, Zinovev E V, Rogachev A V, Kuklin A I and Gordeliy V 2017 Photo-voltage of highly-oriented bacteriorhodopsin in purple membranes: Possibilities for bio solar cells *Optoelectron. Adv. Mater. Commun.* **11** 65–7
[53] Feigin L A and Svergun D I 1987 *Structure Analysis by Small-Angle X-Ray and Neutron Scattering - Springer* ed George W. Taylor
[54] Pernot P, Round A, Barrett R, De Maria Antolinos A, Gobbo A, Gordon E, Huet J, Kieffer J, Lentini M, Mattenet M, Morawe C, Mueller-Dieckmann C, Ohlsson S, Schmid W, Surr J, Theveneau P, Zerrad L and McSweeney S 2013 Upgraded ESRF BM29 beamline for SAXS on macromolecules in solution *J. Synchrotron Radiat.* **20** 660–4
[55] Brennich M E, Kieffer J, Bonamis G, De Maria Antolinos A, Hutin S, Pernot P and Round A 2016 Online data analysis at the ESRF bioSAXS beamline, BM29 *J. Appl. Crystallogr.* **49** 203–12
[56] Volkov V and Svergun D I 2003 Uniqueness of ab-initio shape determination in small-angle scattering *J. Appl. Crystallogr.* **36** 860–4
[57] Petoukhov M V., Franke D, Shkumatov A V., Tria G, Kikhney A G, Gajda M, Gorba C, Mertens H D T, Konarev P V. and Svergun D I 2012 New developments in the ATSAS program package for small-angle scattering data analysis *J. Appl. Crystallogr.* **45** 342–50
[58] Butler P, Alina G, Hernandez R, Doucet M and A. J 2013 SASView for Small Angle Scattering Analysis
[59] Svergun D I 1992 Determination of the regularization parameter in indirect-transform methods using perceptual criteria *J. Appl. Crystallogr.* **25** 495–503
[60] Murugova T N, Vlasov A V, Ivankov O I, Rogachev A V, Soloviov D V, Zhigunov A, Kovalev Y S, Ryzhykau Y L, Zinovev E V, Round A, Gordeliy V I and Kuklin A I 2015 Low resolution structural studies of apoferritin via SANS and SAXS: The Effect of concentration *J. Optoelectron. Adv. Mater.* **17** 1397–402
[61] Grudinin S, Garkavenko M and Kazennov A 2017 Pepsi-SAXS : an adaptive method for rapid and accurate computation of small-angle X-ray scattering profiles *Acta Crystallogr. Sect. D Struct. Biol.* **73** 449–64
[62] de Val N, Declercq J-P, Lim C K and Crichton R R 2012 Structural analysis of haemin demetallation by L-chain apoferritins *J. Inorg. Biochem.* **112** 77–84
[63] Vlasov A, Murugova T, Grudinin S, Ivankov O, Soloviov D, Rogachev A, Round A, Ryzhykau Y, Mishin A, Balandin T, Borschevskiy V, Gordeliy V and Kuklin A 2014 Protein structure and structural ordering versus concentration dependence *FEBS J.* **281** 593